Received: 1 August 2023 | Revised: 27 October 2023 | Accepted: 17 March 2024

DOI: 10.1002/clen.202300187

RESEARCH ARTICLE

CLEAN Soil Air Water

Green synthesis of metal nanoparticles from *Codium macroalgae* for wastewater pollutants removal by adsorption

Muradiye Şahin[1,2] | **Yasin Arslan**[2] | **Fatma Tomul**[3] | **Füsun Akgül**[4] | **Rıza Akgül**[5]

[1]Kırşehir Ahi Evran University, Kırşehir, Turkey

[2]Faculty of Arts and Science, Department of Nanoscience and Nanotechnology, Burdur Mehmet Akif Ersoy University, Burdur, Turkey

[3]Faculty of Arts and Science, Department of Chemistry, Burdur Mehmet Akif Ersoy University, Burdur, Turkey

[4]Faculty of Arts and Science, Department of Molecular Biology and Genetic, Burdur Mehmet Akif Ersoy University, Burdur, Turkey

[5]Food, Agriculture and Livestock Vocational High School, Burdur Mehmet Akif Ersoy University, Burdur, Turkey

Correspondence
Muradiye Şahin, Kırşehir Ahi Evran University, 40100 Kırşehir, Turkey.
Email: muradiye.sahin@ahievran.edu.tr

Funding information
Scientific and Technological Research Council of Türkiye

Abstract

Algae have adsorption properties and reducing agents due to their rich content. In this study, palladium nanoparticles (Pd NP), platinum nanoparticles (Pt NP), and iron oxide nanoparticles (Fe_3O_4 NP) were prepared from *Codium macroalgae* using green synthesis. The structure of the synthesized nanoparticles was elucidated by X-ray diffractometry, Fourier transforms infrared spectroscopy, Brunauer–Emmett–Teller analysis, transmission electron microscopy, ultraviolet-visible spectroscopy and scanning electron microscopy-energy dispersive X-ray spectrometry and their use as nanoadsorbents for the removal of pollutants from aqueous media was investigated in detail. Naproxen (NPX), an anti-inflammatory drug, and the dyes methylene blue (MB) and cresol red (CR) were selected as pollutants for this study. Batch adsorption experiments were conducted using both real wastewater obtained from the Organised Industrial Zone of Isparta Province and synthetic water samples prepared with tap water from Burdur Province and pure water. Under optimum adsorption conditions, Pd NP showed significant efficiency in the real wastewater sample, with an adsorption capacity of 37.19 and 50.03 mg g^{-1} for CR and NPX, respectively, within 150 min. In comparison, Pt NP showed an adsorption capacity of 40.01 mg g^{-1} for MB within the same timeframe. These findings indicate that while Pd NP showed the highest adsorption capacity for both CR and NPX, Pt NP showed the highest adsorption capacity for MB. The Langmuir model and the pseudo-second-order equation were more suitable to describe the adsorption behavior of CR, MB, and NPX. In addition, studies on the desorption and reusability of the nanoadsorbents were carried out under the same optimum experimental conditions.

KEYWORDS
adsorption, algae, green synthesis, metal nanoparticles, pollutant removal

1 | INTRODUCTION

As the sizes of nanoparticles vary between 1 and 100 nm,[1,2] their chemical and physical properties are quite different from their macro and micro counterparts.[3] These small-diameter particles provide advantages, such as higher catalytic reactivity, thermal conductivity, antimicrobial activity and chemical stability, as well as nonlinear optical performance and magnetic properties due to their high surface-to-volume ratio.[1,4] In recent years, nanoparticles have been produced using biological, chemical, physical and hybrid methods.[5] Although

chemical and physical methods are popular for nanoparticle synthesis, they have some important limitations due to environmental risk parameters, the need for different target molecules and surfactants, biodegradation problems and requirements for toxic chemicals.[6–8] Therefore, nanoparticles obtained by the green synthesis method attract attention because of some advantages, such as targeting the active substance to the desired region, increased bioavailability, controlled release, reduction in side effects, low-dose effect, nontoxicity, high stability, environmentally friendly, stable product, biocompatible, and being economical.[5,7,9] Using the green synthesis, nanoparticles are produced by fungi, bacteria, yeast, plant extracts, algae and biomolecules.[4,9,10] In principle, macroalgae, microalgae, and cyanobacteria, which are defined as algae in general terminology, are photosynthetic organisms that live in single cell form or colonies in fresh, salty, and carbonated water sources and soil.[11] Macroalgae and microalgae are defined as multicellular and unicellular eukaryotic organisms, respectively, while cyanobacteria are defined as prokaryotic microorganisms.[6,12] Because they are periodically exposed to extreme environmental conditions, such as high temperature, high UV radiation, and high salinity due to their habitat, they synthesize various intracellular and extracellular metabolites to protect themselves.[13] Furthermore, they also synthesize polysaccharides, fatty acids, vitamins, pigments (carotenoids, phycobiliproteins, chlorophyll pigments), and phenolic components. Because they have a rich cellular content, the interest in algae has intensified in recent years and they have been used for different purposes in many commercial areas. It is known that these active compounds also act as both reducing and stabilizing agents to produce nanoparticles by the green synthesis method.[14–16]

In general, increasing population, environmental changes and industrial applications with the developing industry negatively affect the quality of water and cause increasing water pollution.[17] Some pollutants, such as dyes, drugs, disinfectants, imaging agents, laundry detergents, surfactants, pesticides, preservatives, food additives, and personal care products pose a serious threat to the environment and human health on a global scale.[18,19] These pollutants pass into the environment during their manufacture,[20] through sewage,[21–23] land applications, municipal waste, and improper disposal of unused or expired drugs.[24] Among these pollutants, naproxen (NPX) more adversely affects particularly some organisms, such as larvae and embryos.[25,26] Furthermore, wastewater containing dyestuffs causes toxic and carcinogenic effects for living things in the receiving environment because they directly affect light transmission and oxygen solubility.[27,28] Therefore, the removal of NPX and some dyes from aqueous media is crucial and remarkable. In principle, adsorption is one of the most preferred methods to remove pollutants from aqueous media due to its low cost, flexibility, easy design and application, having no harmful waste materials and effective removal potential for other methods, such as chlorination, coagulation/sedimentation, ozonation, oxidation, and biofiltration.[29–31]

In this study, Fe_3O_4 NP, Pd NP, and Pt NP were prepared using *Codium macroalgae* extract by the green synthesis method, which is an environmentally friendly, cost-effective, and efficient method for nanoparticle biosynthesis. As far as we can ascertain, *Codium macroalgae* extract has been used for the first time in the synthesis of the above nanoparticles using green synthesis and it is the first time that it has been used as an adsorbent in the removal of MB, CR, and NPX from real wastewater. In this study, the removal capacity of three different magnetic and metallic nanoparticles prepared from *Codium macroalgae* for CR, MB, and NPX from both tap water and real wastewater matrices was investigated in detail in which *Codium macroalgae* itself can adsorb only 37% of MB in 24 h. Experimental results showed that all nanoparticles provided removal in a shorter time and with a higher capacity compared to *Codium macroalgae* itself.

2 | EXPERIMENTAL

2.1 | Materials and chemicals

The chemicals such as $FeSO_4 \cdot 7\,H_2O$ (iron(II) sulphate heptahydrate), $FeCl_3 \cdot 6\,H_2O$ (iron(III) chloride hexahydrate), $Pd(NO_3)_2 \cdot 2\,H_2O$ (palladium(II) nitrate dehydrate), $H_2PtCl_6 \cdot 6\,H_2O$ (hexachloroplatinic acid hexahydrate), NaCl (sodium chloride), and NaOH (sodium hydroxide) were obtained from Sigma-Aldrich and $C_{21}H_{17}NaO_5S$ (cresol red) and HCl (hydrochloric acid) were obtained from Merck. On the other hand, $C_{14}H_{13}NaO_3$ (sodium naproxen) was obtained from Acros Organics and $C_{16}H_{18}ClN_3S$ (methylene blue) was obtained from Fluka. The real wastewater sample was obtained from Isparta City Organised Industrial Zone. All materials used were of analytical reagent grade and were used as received without any purification. High purity water (18 MΩ cm) obtained from the PURIS pure water system (PURIS, Expe-UP series) was used for all solutions in the experimental studies.

2.2 | Characterization

In order to explain both the morphology and the chemical structures of the nanoparticles, UV-Vis (Shimadzu UV-1800, from 200 to 1100 nm), Fourier transform infrared spectroscopy (FTIR, Perkin Elmer Fronter), X-ray diffraction (XRD, Bruker D8 Advance, K_α radiation with about 2θ: 10°–90°), transmission electron microscopy (TEM, Jeol Jem-1400 Plus, TEM-120kV), scanning electron microscopy-energy dispersive X-ray spectrometry (SEM-EDX, Carl Zeiss EVO-LS 10), and N_2 adsorption isotherms (Quantachrome Quadrasorb SI, 77K, P/P_0- 0.99) were used. Furthermore, the common drift method was used to determine the pH (pH_{pzc}) of the nanoparticles at the zero charge point.[31–33] For this, 50 mL of 0.01 M NaCl solution was placed in a closed flask. The pH value was adjusted to 2–12 by adding 0.1 M HCl and/or 0.1 M NaOH solutions. Then, 0.05 g of each nanoparticle was added separately and mixed at room temperature. The pH change was determined after 24 h using a pH meter (Thermo Scientific, Orion 3 Star) and plotted against the initial pH value. The pH_{pzc} values were found from the cut-off point.

2.3 | Preparation of macroalgae biomass

The macroalga used in this study was identified by looking at features, such as thallus structure, color, and branching shape. Morphometric characteristics were also compared with data reported in the literature[34] and named as *Codium fragile* (Suringar) Hariot.

Macroalgae samples were collected manually from the shores of the Çanakkale Strait, Turkey (40°09′37.7"N, 26°24′11.7"E), from the zone where the water depth is between 10 and 50 cm. Collected samples were placed in bags with seawater and transported to the laboratory by cold chain. Epiphytes and macroalgal debris were removed. Afterward, the algal biomass was washed three times with high purity water, spread on blotting paper, and dried in an oven at 45°C. The dry biomass was pulverized, homogenized and sieved to obtain 100–200 μm particles.

2.4 | Synthesis of Fe_3O_4, Pd, and Pt nanoparticles

The nanoparticles were synthesized from the macroalgae extract using the extracellular method. To prepare the algae extract, 1 g of *Codium macroalgae* was weighed and crushed in a mortar. It was then stirred in 50 mL of ultrapure water at 500 rpm for 3 h at room temperature and then filtered using Whatman No 1 filter paper. For Fe_3O_4 NP, 100 mL solution containing 0.81 g $FeCl_3 \cdot 6\,H_2O$ and 0.56 g $FeSO_4 \cdot 7\,H_2O$ and 10 mL algae extract were mixed. On the other hand, 100 mL of 0.1 M $Pd(NO_3)_2 \cdot 2\,H_2O$ and 100 mL of 0.1 M $H_2PtCl_6 \cdot 6\,H_2O$ solutions were separately mixed with 10 mL of algae extract to obtain Pd NP and Pt NP, respectively. These mixtures were then incubated in an oven at 45°C for 2 h and kept in the dark during overnight. While magnetic Fe_3O_4 NP was separated from the filtrate using a magnet, both Pd NP and Pt NP were separated using a Whatman No 1 filter paper and stored in an oven at 50°C until use.

2.5 | Adsorption experiments

Batch adsorption was used to adsorb NPX, MB, and CR onto nanoadsorbents. For this purpose, 25 mg L^{-1} of NPX, MB, and CR were spiked separately into the tap water obtained from Burdur city in Turkey as the tap water used does not contain NPX, MB, and CR and adsorption studies have been performed with optimal experimental parameters. 25 mg adsorbent was mixed with 50 mL tap water containing each 25 mg L^{-1} of NPX, MB, and CR and stirred for for 2 h at 250 rpm. The tap water characteristics are shown in Table S1. The concentrations of NPX, MB, and CR in the solution were calculated using UV-Vis spectrophotometry based on their specific calibration plots drawn at 272, 664, and 435 nm, respectively. Furthermore, isothermal studies were carried out with initial concentrations ranging from 2.5 to 200 mg L^{-1} for NPX, MB, and CR for 2 h at 298 K and adsorption kinetic studies were carried out between 2 and 150 min at 298 K. All experimental studies were carried out using spiked tap water samples. Finally, adsorption, desorption, and reusability studies were performed on real wastewater samples under the same optimum experimental conditions. The characteristics for the wastewater are shown in Table S2.

3 | RESULTS AND DISCUSSION

3.1 | Characterization of metal and metal oxide nanoparticles

Fe_3O_4 NP, Pt NP, and Pd NP were verified by their characteristic peaks in UV-Vis spectra (Figure 1a).[35–39] The pH_{pzc} values of Fe_3O_4 NP, Pt NP, and Pd NP were determined to be 5.44, 6.02, and 5.81, respectively (Figure 1b). The studies for CR and NPX were carried out at pH 5, which is below the pH_{pzc} value for all nanoparticles. In principle, when pH < pH_{pzc}, the adsorbent surface is positive and this positive surface can easily adsorb anions.[40] For this reason, MB adsorption was performed at pH 8 which is >pH_{pzc}.

The FTIR results of Fe_3O_4 NP, Pd NP, Pt NP, and Codium extract are shown comparatively in Figure 2a. The wide flat peak seen in the spectrum at 3465–3220 cm^{-1} for the Codium extract can be assigned to asymmetric vibration of -NH and -OH originating from protein, polysaccharide, and polyphenol in algae. This band is narrowed in Pt NP and is not observed for the other nanoparticles. Furthermore, the sharp peak seen in the spectrum at 1100–1230 cm^{-1} for Codium extract is the -COC vibrational band of the polysaccharide found in algae. A narrowing of this band was observed for all nanoparticles. Other peaks seen in the spectrum at 2920 cm^{-1} for Codium extract are corresponding to the –CH and $–CH_2$ aliphatic group stretching band, at 1730 cm^{-1} corresponding to the C = O ester or fatty acid vibration band, at 1510 cm^{-1} corresponding to the polyphenol skeletal (aromatic) band, at 1435 cm^{-1} corresponding to the –CH aliphatic bending group, at 875 cm^{-1} corresponding to bending -C = O inorganic carbonate band and at 690 cm^{-1} corresponding to the –CH out-of-plane aromatic band, respectively. FTIR analysis revealed that polysaccharides, phenolic compounds, and fatty acids present in the Codium extract served as both reducing and stabilizing agents for the synthesis of the targeted nanoparticles.[14–16]

The XRD spectra of *Codium macroalgae*, Fe_3O_4 NP, Pd NP, and Pt NP are shown in Figure 2b. As seen from the XRD spectra of Fe_3O_4 NP, six crystal structure peaks (orthorhombic) at 220, 311, 400, 422, 511, and 440 correspond to $2\theta = 30.06°, 35.47°, 43.30°, 53.48°, 57.06°$, and 63.70°, respectively (JCPDS Card No. 76–0957). The particle size of Fe_3O_4 NP was determined to be 14.15 nm based on $2\theta = 35.47°$ in the XRD spectrum of Fe_3O_4 NP using the Debye–Scherrer equation:

$$D = K\lambda/\beta\cos\theta, \quad (1)$$

where D is the nanoparticles crystalline size, K represents the Scherrer constant (0.98), λ denotes the wavelength (1.54), β denotes the full width at half maximum (FWHM).

As seen from the XRD spectra of Pd NP, four crystal structure peaks (hexagonal) at 111, 200, 220, and 311 correspond to 2θ = 40.01°, 44.80°, 63.41°, and 71.27°, respectively (JCPDS Card No. 72–0710).

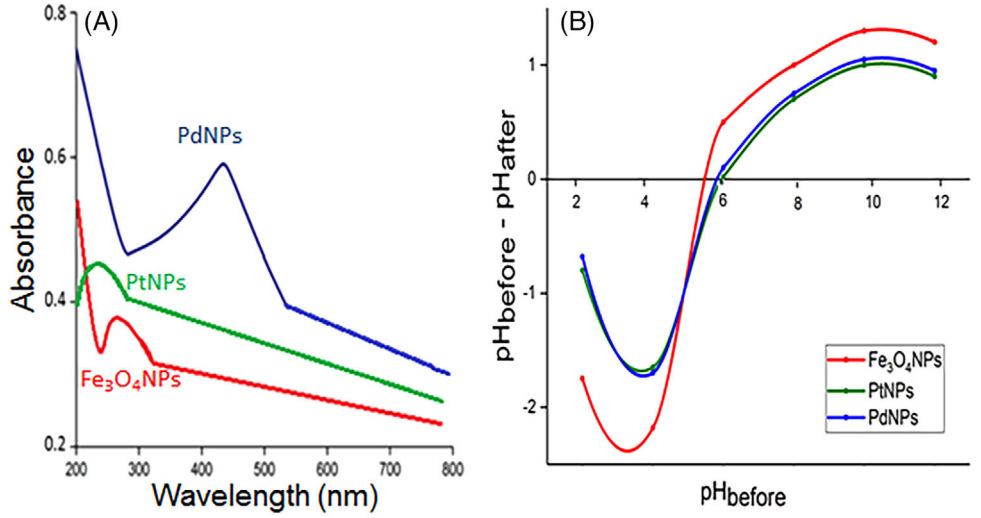

FIGURE 1 (a) UV-Vis spectra of Fe_3O_4 NP, Pd NP, and Pt NP (10 mL Codium extract, 0.56 g $FeSO_4 \cdot 7\ H_2O$, 0.81 g $FeCl_3 \cdot 6\ H_2O$, 25°C, 0.1 M $Pd(NO_3)_2 \cdot 2\ H_2O$ and 0.1 M $H_2PtCl_6 \cdot 6\ H_2O$) and (b) pH_{pzc} of the adsorbents (25 mg nanoparticles, 25 mL 0.01 M NaCl, 25°C and 24 h)

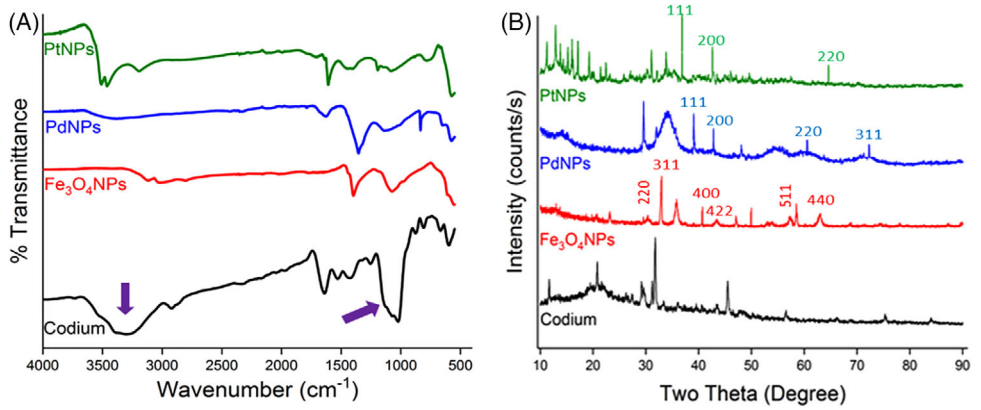

FIGURE 2 (a) FTIR and (b) XRD spectra of macroalgae and nanoparticles.

The particle size of Pd NP was determined to be 11.38 nm based on $2\theta = 40.01°$ in the XRD spectrum of Pd NP using the Debye–Scherrer equation. As seen from the XRD spectra of Pt NP, three crystal structure peaks (cubic) at 111, 200, and 220 correspond to $2\theta = 40.01°$, 46.70°, and 68.10°, respectively (JCPDS Card No. 87–0767). The particle size of Pt NP was determined to be 15.97 nm based on $2\theta = 40.01°$ in the XRD spectrum of Pt NP using the Debye–Scherrer equation.

Both the surface and crystalline structures, elemental compositions, sizes and shapes of the nanoparticles were determined from the SEM-EDX and TEM analyses shown in Figure 3. Based on the TEM results, it was found that the average sizes of Fe_3O_4 NP, Pd NP, and Pt NP were 14.23 ± 0.08, 11.48 ± 0.13, and 15.75 ± 0.21 nm, respectively, and all the nanoparticles showed monodispersed distribution and had spherical crystal structure. The FTIR spectra in Figure 2a confirm that some elements, such as Mg, Na, C, and O observed in the EDX spectra of the nanoparticles (Figure 3), originated from the algae extract. The element Cl observed in the EDX spectra of both Fe_3O_4 NP and Pt NP is thought to be due to metal salts. The SEM images showed an irregular oval and spherical morphology as well as agglomeration of the nanoparticles.

TABLE 1 Textural properties and particle size of nanoadsorbents.

Property	Fe_3O_4 NP	Pd NP	Pt NP
Specific (BET) surface area (S_{BET}, $m^2\ g^{-1}$)	6.356	99.613	7.938
Total pore volume (V_{total}, $cm^3\ g^{-1}$)	0.036	0.058	0.037
Average pore diameter (BJH) (L, nm)	18.391	3.100	3.874

The pore diameter, total pore volume, and surface area of the synthesized nanoparticles were calculated by both Barrett–Joyner–Halenda (BJH) and Brunauer–Emmett–Teller (BET) methods using the N_2 adsorption isotherm (Figure 4). As can be seen in Figure 4, Fe_3O_4 NP and Pt NP probably follow the IUPAC classified Type III isotherm, which is related to the slit-like pores between parallel layers. Pd NP follows the Type II isotherm classified by IUPAC; possibly related to mesopores.[41] The obtained pore diameter (L), surface area (S_{BET}) and total pore volume (V_{total}) data are shown in Table 1. As can be seen in Table 1, Pd NP has the largest surface area, although the average pore size is the smallest. The pore diameters of Fe_3O_4 NP, Pd NP, and Pt NP are shown in Table 1, with average pore diameters approximately

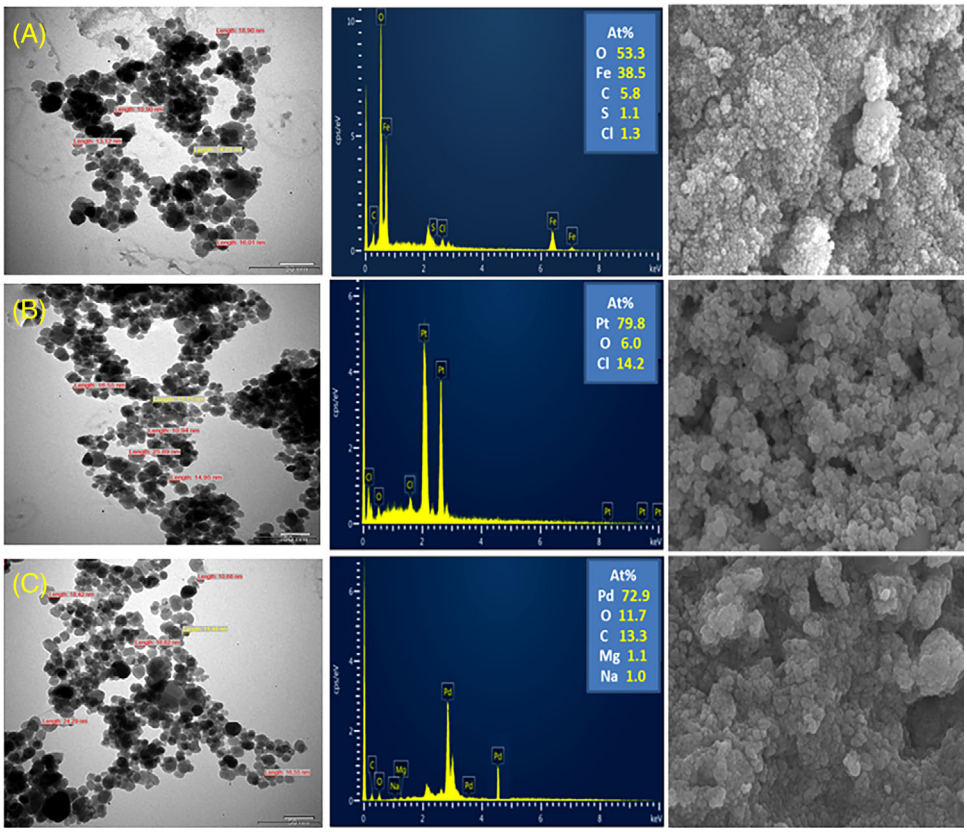

FIGURE 3 From left to right, TEM, EDX and SEM images: (a) Fe_3O_4 NP, (b) Pt NP, and (c) Pd NP.

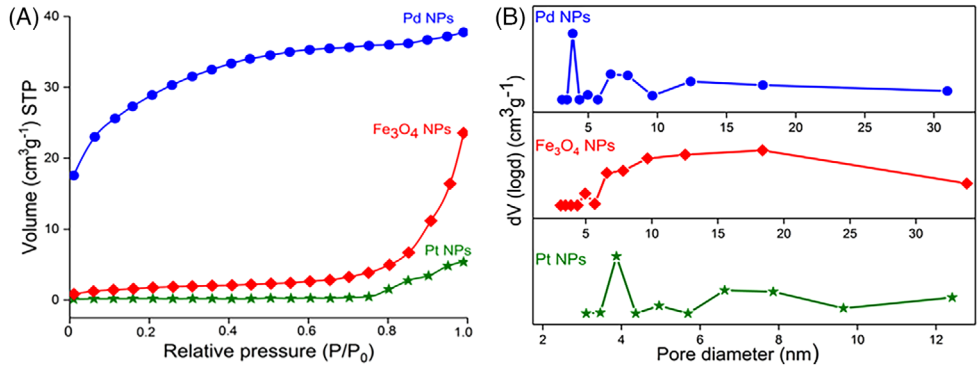

FIGURE 4 (a) N_2 adsorption isotherms, (b) BJH analysis of pore size distribution for Fe_3O_4 NP, Pd NP, and Pt NP.

equal to 18.39, 3.10, and 3.87 nm, respectively. It is understood from Figure 4b that the nanoparticles are mesoporous.

3.2 | Removal efficiency of nanoparticles for NPX, MB, and CR from tap water

The adsorption results of 25 mg L^{-1} CR, MB, and NPX solutions (50 mL) by separately using 25 mg of Fe_3O_4 NP, Pd NP, and Pt NP at room temperature are shown in Figure 5a–c. While the % removal of CR with Fe_3O_4 NP, Pd NP, and Pt NP at 2 h were found to be 39%, 83.5%, and 71%, respectively, those of MB with Fe_3O_4 NP, Pd NP, and Pt NP were found to be 43%, 76%, and 90%, respectively. Furthermore, the percentage removal of NPX with Fe_3O_4 NP, Pd NP, and Pt NP at 2 h were found to be 45%, 95%, and 82%, respectively. On the other hand, MB dye removal was found to be 37% at 24 h using Codium algae only. Pd NP showed the highest adsorption capacity for both CR and NPX, while Pt NP showed the highest adsorption capacity for MB. All the experimental studies were repeated with both high purity water and tap water containing 25 mg L^{-1} of NPX, MB, and CR and the same adsorption capacities were obtained for all the nanoadsorbents, shown in Figure S1. This experimental result showed that foreign ions in tap

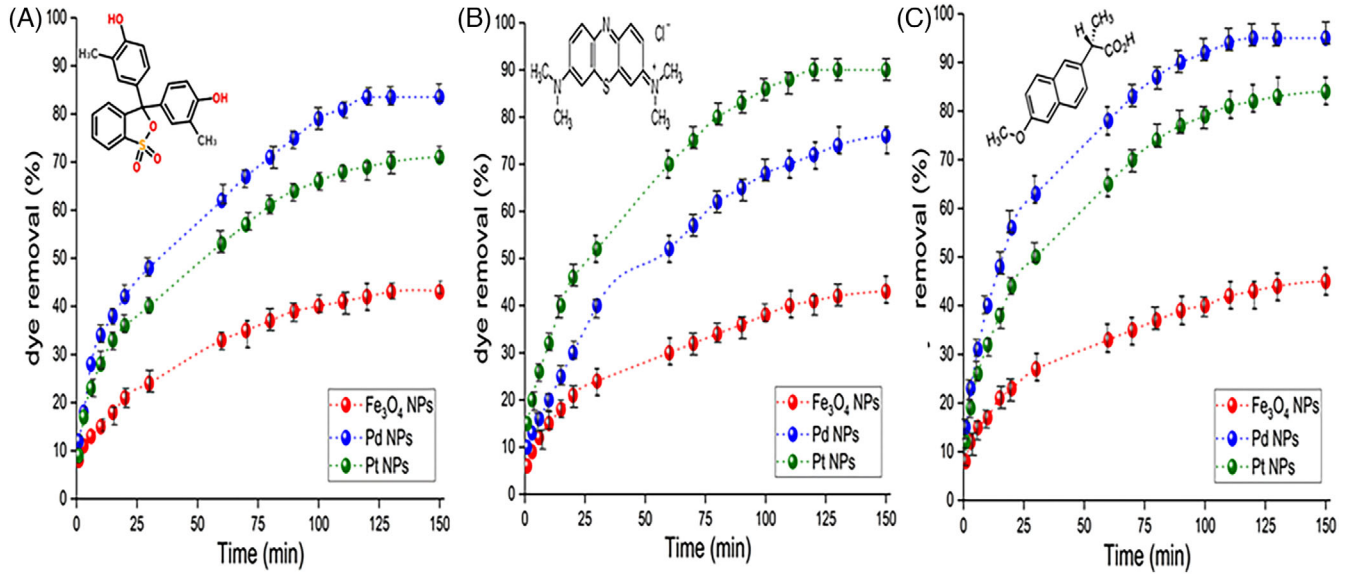

FIGURE 5 Comparative removal efficiency for (a) CR, (b) MB, and (c) NPX using Fe_3O_4 NP, Pd NP, and Pt NP (initial dye/drug concentration: 25 mg L^{-1}, adsorbent dosage: 25 mg in 50 mL, $T = 298$ K)

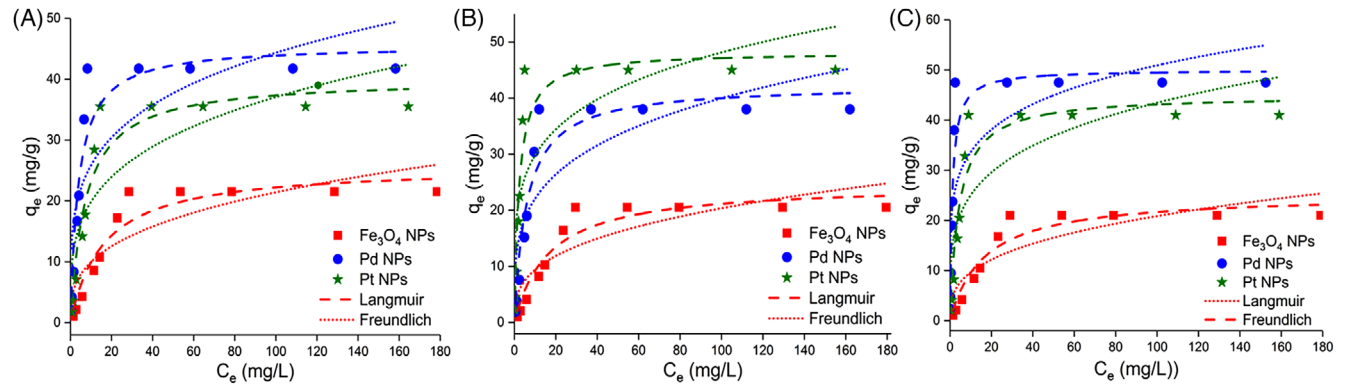

FIGURE 6 Adsorption isotherm models of (a) CR, (b) MB, and (c) NPX onto Fe_3O_4 NP, Pd NP, and Pt NP (adsorption conditions: 0.025 g NP in 50 mL, 2.5–200 mg L^{-1}, 298 K, 120 min).

water did not have a negative effect on the removal of NPX, MB, and CR. Pd NP had the highest removal efficiency for both CR and NPX and the results are in agreement with the BET analysis. According to the BET analysis results, Pd NP has the highest surface area and pore volume.

The two most commonly used adsorption isotherms, such as the Langmuir and Freundlich isotherm models, were used to analyze the equilibrium adsorption of CR, MB, and NPX shown in Figure 6, respectively. On the other hand, pseudo-first order (Lagergren), pseudo-second order (Ho-McKay) and Elovich kinetic models were applied to study the adsorption kinetics of CR, MB, and NPX (Figure 7). The basic equations of the two isothermal and kinetic models used are given in Table 2. The constants and equations were explained in detail in the literature.[42,43]

Since the R^2 value of the line drawn according to the Langmuir model of CR, MB, and NPX adsorption by Fe_3O_4 NP, Pd NP, and Pt NP at 298 K is closer to 1 than the R^2 value drawn according to the Freundlich model (Table 3), it is seen that the adsorption equilibrium model is more suitable for the Langmuir model. Based on the experimental results, it is understood that the adsorption energy of all areas on the adsorbent surface is constant and the adsorbent surface is homogeneous. Therefore, it is found that the adsorption takes place in a single layer. When the maximum adsorption capacity of adsorbents is compared, it is seen that while Pd NP is optimal for both CR and NPX removal, Pt NP is most appropriate for MB removal.

TABLE 2 Isotherm and kinetic mathematical models

Isotherm/Kinetic model	Equation
Langmuir	$q_e = \frac{q_m K_L C_e}{1+K_L C_e}$
Freundlich	$q_e = K_F C_e^{1/n}$
Pseudo-first order	$q_t = q_e (1 - e^{-k_1 t})$
Pseudo-second order	$q_t = \frac{q_e^2 k_2 t}{1+q_e k_2 t}$
Elovich	$q_t = \frac{1}{\beta} \ln(1 + \alpha\beta t)$

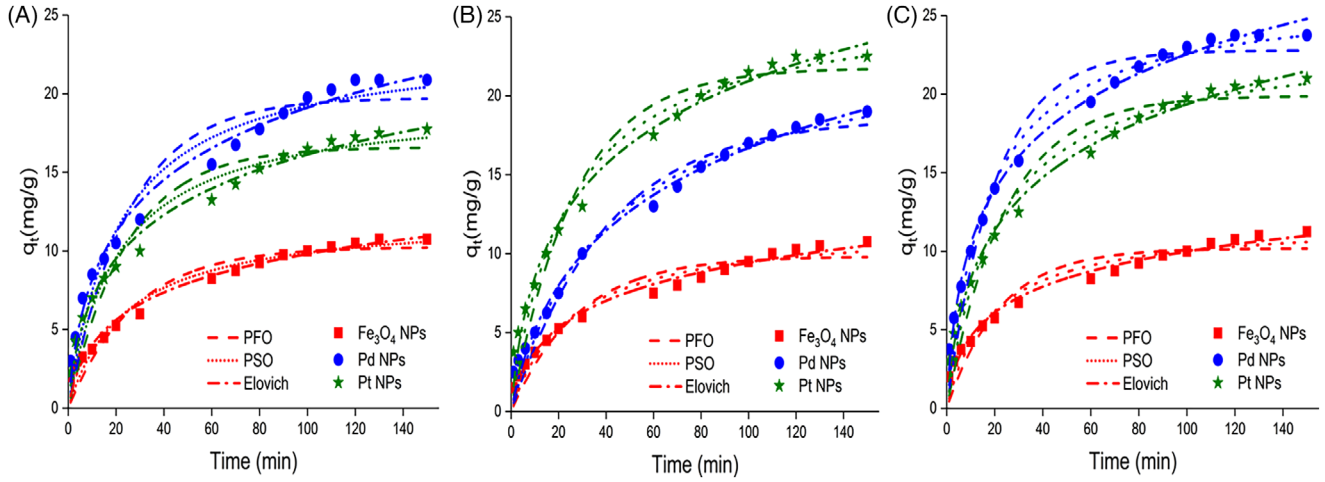

FIGURE 7 Kinetic models for adsorption of (a) CR, (b) MB, and (c) NPX onto Fe_3O_4 NP, Pd NP, and Pt NP (adsorption conditions: 0.025 g NP in 50 mL, initial dye/drug concentration 25 mg L^{-1}, 150 min).

TABLE 3 Isotherm models constants for CR, MB, and NPX adsorption on Fe_3O_4 NP, Pd NP, and Pt NP.

		CR			MB			NPX		
Isotherm parameter		**Fe_3O_4 NP**	**Pd NP**	**Pt NP**	**Fe_3O_4 NP**	**Pd NP**	**Pt NP**	**Fe_3O_4 NP**	**Pd NP**	**Pt NP**
Langmuir	q_m (mg g^{-1})	25.75	45.62	40.08	24.65	42.37	48.22	25.20	50.03	44.99
	K_L (L mg^{-1})	0.06	0.25	0.14	0.06	0.17	0.43	0.061	0.90	0.23
	R^2	0.93	0.92	0.92	0.93	0.92	0.92	0.92	0.91	0.92
Freundlich	K_F (mg g^{-1})/(mg L^{-1})^n	4.64	15.06	10.60	4.34	12.17	18.42	4.49	22.22	14.41
	n	0.33	0.51	0.27	0.34	0.26	0.21	0.33	0.18	0.24
	R^2	0.77	0.70	0.73	0.77	0.72	0.69	077	0.67	0.71

TABLE 4 Kinetic modeling the experimental data of CR, MB, and NPX on Fe_3O_4 NP, Pd NP, and Pt NP.

		CR			MB			NPX		
Kinetic model parameter		**Fe_3O_4 NP**	**Pd NP**	**Pt NP**	**Fe_3O_4 NP**	**Pd NP**	**Pt NP**	**Fe_3O_4 NP**	**Pd NP**	**Pt NP**
PFO	q_e (mg g^{-1})	10.25	19.73	16.60	9.829	18.61	21.76	10.18	22.78	19.90
	$k_1 \times 10^{-3}$ (min^{-1})	0.036	0.040	0.041	0.036	0.025	0.037	0.045	0.050	0.041
	R^2	0.934	0.929	0.933	0.930	0.971	0.952	0.906	0.957	0.952
PSO	q_e (mg g^{-1})	12.29	23.33	19.59	11.83	23.81	26.09	11.88	26.37	23.55
	$k_2 \times 10^{-3}$ (g (mg × min)$^{-1}$)	0.003	0.002	0.002	0.003	0.001	0.002	0.005	0.002	0.002
	R^2	0.978	0.985	0.989	0.986	0.989	0.987	0.983	0.994	0.992
Elovich	β (mg g^{-1})	0.356	0.191	0.229	0.361	0.154	0.165	0.397	0.178	0.188
	α (g mg^{-1} × min)	0.898	1.970	1.715	0.802	0.788	1.860	1.301	3.069	1.987
	R^2	0.958	0.963	0.967	0.963	0.982	0.974	0.949	0.983	0.977

PFO: pseudo-first order; PSO: pseudo-second order.

The calculated kinetic parameters for the three models are shown in Table 4. The high regression coefficients of the pseudo-second-order kinetic model indicate that the experimental results for CR, MB, and NPX removal are well explained by this model. The regression coefficients close to 1 for all pollutants show the applicability of this model. Therefore, it can be concluded that the adsorption process of CR, MB, and NPX is controlled by chemisorption.[44]

3.3 | Adsorption, desorption, and reusability in real wastewater

Because the concentrations of CR, MB, and NPX in the wastewater samples collected from Isparta Organised Industrial Zone were below detection limit, 25 mg L^{-1} of each pollutant was spiked into the wastewater separately. Adsorption, desorption and reusability studies were

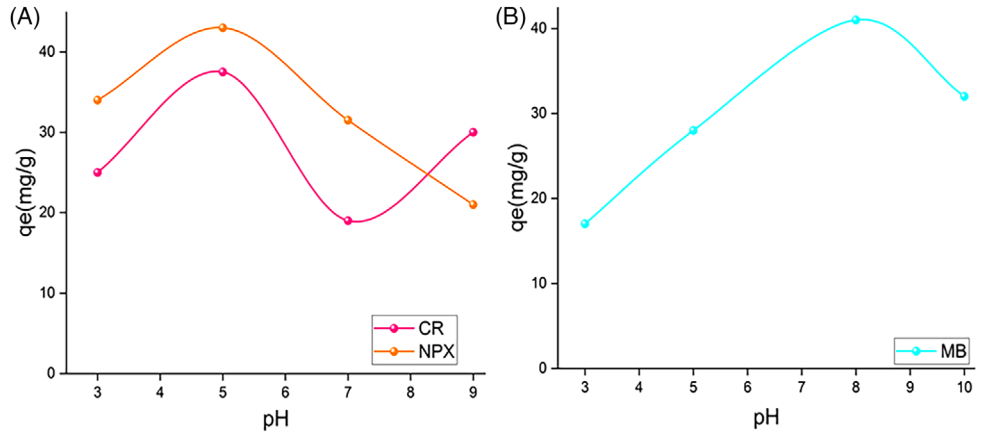

FIGURE 8 Effect of initial pH for the removal of both (a) CR and NPX with Pd NP and (b) MB with PtNP (adsorption conditions: 0.025 g NP in 50 mL, initial dye/drug concentration 25 mg L^{-1}, 298 K, 150 min).

TABLE 5 A comparison of the adsorptive capacity of synthesized nanosorbent with those announced in the literature for degradation different pollutants.

Pollutant	Adsorbent	Adsorption capacity (mg g^{-1})	Time (min)	Reference
Tetracycline	Fe/Ni NP	61.89	90	[45]
Diclofenac	Cu NP	21.60	90	[46]
Naproxen	Cu NP	19.6	90	[46]
Naproxen	Natural clay	37	240	[49]
Reactive red-198	Alumina/carbon nanotube	44.32	150	[48]
Cresol red	Orange peel	14	1440	[49]
Methyl orange	Fe_3O_4 NP	132	60	[31]
Methylene blue	Banana peel	20.8	1440	[49]
Methyl orange	Graphene oxide	16.83	100	[50]
Naproxen	Pd NP	41	150	Present study (real wastewater)
Cresol red	Pd NP	37.19	150	Present study
Methylene blue	Pt NP	40.01	150	Present study
Naproxen	Pd NP	50.03	120	Present study (tap water)
Cresol red	Pd NP	45.62	120	Present study
Methylene blue	Pt NP	48.22	120	Present study

carried out using Pd NP as the adsorbent for both CR and NPX and Pt NP for MB. Firstly, adsorption studies were carried out with wastewater samples in the pH range of 2 to 10 to determine the appropriate pH (Figure 8).

CR removal studies from wastewater were carried out at pH 5, which gives the best results. The pH_{pzc} value for Pd NP was found to be 5.81 (Figure 1b). Since the selected pH is lower than the pH_{pzc} value, the surface of the nanoadsorbent is positively charged and an electrostatic attraction force is formed with $—SO_3^-$ and $—O^-$ ions of CR. On the other hand, since the pK_a value of CR is 8.2 which is higher than the pH of the solution, electrostatic repulsion occurs and it is believed that the adsorption equilibrium time is prolonged. In this case, n-π^*, π-π^* electron donor–acceptor (EDA) forces arising from —S = O and —C = C groups are thought to be more effective in adsorption. From the results obtained, it was concluded that Pd NP at basic

TABLE 6 Desorption efficiency (%) of CR, MB, and NPX from Pd NP and Pt NP.

Desorption agent	Desorption efficiency (%)	Adsorbent	Pollutant
Methanol	92	Pd NP	CR
	96		NPX
	95	Pt NP	MB
Ethanol	95	Pd NP	CR
	98		NPX
	95	Pt NP	MB
1 M NaOH	-	Pd NP	CR
	-		NPX
	5	Pt NP	MB

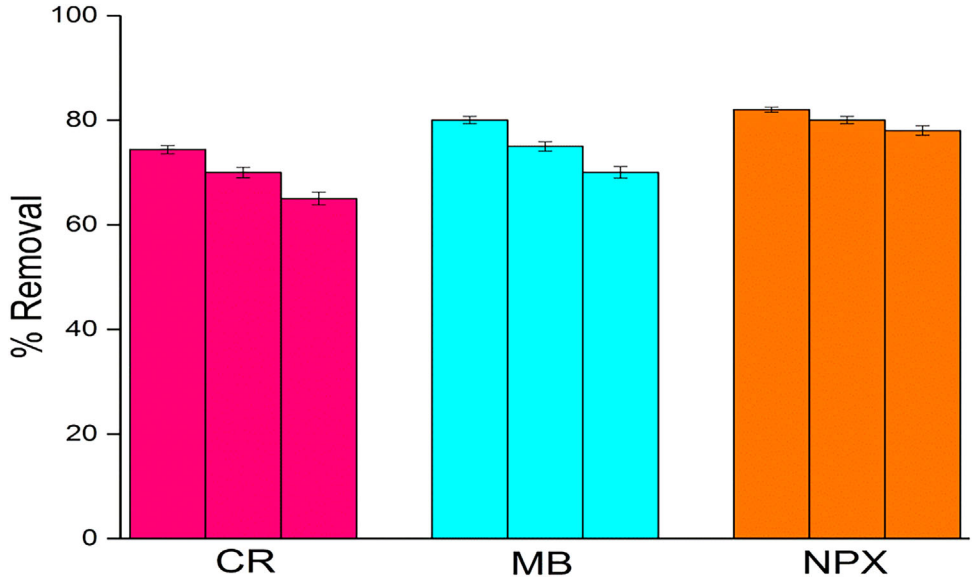

FIGURE 9 Reusability of Pd NP for CR and NPX removal and Pt NP for MB removal for three cycles (from 1st to 3rd from left to right, respectively).

pH has low adsorption capacity for NPX removal. The highest adsorption capacity for NPX removal was also obtained at pH 5. Since the pH is lower than the pH_{pzc} value of Pd NP and higher than the pK_a value of NPX, it becomes anionic, and since the nanoparticle surface is positively charged, electrostatic attraction force occurs with the positively charged nanoparticle surface. In addition other interactions can still be effective (H-bond and aromatic ring-induced π-π^* interaction). Figure 8b shows that the adsorption capacity of MB is highest at pH 8, which is higher than both $pK_a = 2.6$ of MB and $pH_{pzc} = 6.02$ of Pt NP. Therefore, the surface of the nanosorbent is negatively charged and the adsorption is due to both the electrostatic attraction of MB with N^+ ions and the n-π^*, π-π^* interactions of -CN and aromatic ring -C = C groups on the nanoparticle surface.

The removal percentage of CR, MB, and NPX from wastewater was 74.38%, 80.01%, and 82%, respectively, which was lower than the removal percentage from tap water (83.5%, 90%, and 95%). This may be due to the different pollutants and constituents present in the wastewater.

A comparison of the adsorptive capacity of the synthesized nanosorbents with other materials reported in the literature is shown in Table 5.

As shown in Table 5, while the adsorption capacity of both Cu NP and natural clay for NPX was 19.60 mg g^{-1} at 90 min and 37 mg g^{-1} at 240 min, respectively,[46,47] the adsorption capacity of Pd NP prepared using *Codium macroalgae* extract for NPX was 50.03 mg g^{-1} at 120 min. Furthermore, 14 mg g^{-1} of CR was removed at 1440 min by using orange peel as an adsorbent,[49] whereas 45.62 mg g^{-1} of CR was removed at 120 min by using Pd NP prepared using *Codium macroalgae* extract. Furthermore, while the adsorption capacity of banana peel for MB was found to be 20.8 mg g^{-1} at 1440 min,[49] the adsorption capacity of Pt NP prepared using *Codium macroalgae* extract for MB was 48.22 mg g^{-1} at 120 min. Comparing the present study with some other studies in the literature, the removal of NPX, CR, and MB was achieved with higher efficiency at lower times as shown in Table 5.

In terms of both economics and sustainability, desorption and reusability studies are important parameters for evaluating potential environmental applications. For this reason, desorption studies of CR, MB, and NPX were investigated using different solvents and the results are shown in Table 6. To investigate the reusability of the nanoadsorbents, the adsorption/desorption studies were repeated three times and the results are shown in Figure 9. As shown in Figure 9, the adsorbent has a stable and active structure and there was a slight decrease in the adsorption capacities.

4 | CONCLUSIONS

Magnetic Fe_3O_4 and both Pd and Pt metallic nanoparticles were first prepared using *Codium macroalgae* extract by green synthesis and successfully used for the removal of NPX, CR, and MB from aqueous media. The optimum experimental conditions for the removal of NPX, CR, and MB with the highest efficiency in the shortest time were determined, and kinetic studies were carried out. Based on the experimental results obtained with both high purity water and tap water, ions present in tap water did not have a negative effect on the removal of NPX, MB, and CR. It can be concluded that the adsorption process of CR, MB, and NPX was controlled by chemical adsorption due to the suitability of pseudo-second-order kinetic model. The Langmuir adsorption model is more suitable than the Freundlich model for the adsorption of CR, MB, and NPX and it is found that the adsorption takes place in a single layer. While 37% of MB was removed after 24 h using *Codium macroalgae* only, 90% of MB was removed after 2 h using Pt NP. Furthermore, while the adsorption capacity of Pd NP is the

highest for both CR (83.5%) and NPX (95%), that of Pt NP is the highest for MB (90%). The adsorption, desorption and reusability studies were investigated in real wastewater samples collected from Isparta City Organised Industrial Zone and it was found that the synthesized nanoparticles can be used in real wastewater despite a small capacity loss. Among the synthesized nanoparticles, Pd NP can be used as an effective nanoadsorbent for the removal of pollutants from aqueous media at acidic pH. Therefore, these results show that metallic nanoadsorbents obtained by using *Codium macroalgae* extract are preferred adsorbents for the removal of organic pollutants from aqueous media.

AUTHOR CONTRIBUTIONS

Muradiye Şahin: Investigator; performing the experiment; writing—original draft; visualization. Yasin Arslan: Conceptualization; writing—review & editing; supervision; funding acquisition. Fatma Tomul: Resources; software. Füsun Akgül: Algae supply; preparation of macroalgae biomass; writing—original draft. Rıza Akgül: Algae supply; preparation of macroalgae biomass; writing—original draft.

ACKNOWLEDGMENTS

The authors wish to thank open access funding provided by the Scientific and Technological Research Council of Türkiye (TÜBİTAK).

CONFLICT OF INTEREST STATEMENT

The authors declare that they have no known competing financial interests or personal relationships that could have appeared to influence the work reported in this paper.

DATA AVAILABILITY STATEMENT

Data will be made available on request.

ORCID

Muradiye Şahin https://orcid.org/0000-0002-5445-6682

REFERENCES

1. McNamara, K., & Tofail, S. A. M. (2017). Nanoparticles in biomedical applications. *Advances in Physics: X*, *2*(1), 54–88.
2. Sharma, A., Sharma, S., Sharma, K., Chetri, S. P. K., Vashishtha, A., Singh, P., Kumar, R., Rathi, B., & Agrawal, V. (2016). Algae as crucial organisms in advancing nanotechnology: A systematic review. *Journal of Applied Phycology*, *28*, 1759–1774.
3. Farre, M., Gajda-Schrantz, K., Kantiani, L., & Barceló, D. (2009). Ecotoxicity and analysis of nanomaterials in the aquatic environment. *Analytical and Bioanalytical Chemistry*, *393*(1), 81–95.
4. Patel, V., Berthold, D., Puranik, P., & Gantar, M. (2015). Screening of cyanobacteria and microalgae for their ability to synthesize silver nanoparticles with antibacterial activity. *Biotechnology Reports*, *5*, 112–119.
5. Li, X., Xu, H., Chen, Z. S., & Chen, G. (2011). Biosynthesis of nanoparticles by microorganisms and their applications. *Journal of Nanomaterials*, *2011*, 16.
6. Agarwal, P., Gupta, R., & Agarwal, N. (2019). Advances in synthesis and applications of microalgal nanoparticles for wastewater treatment. *Journal of Nanotechnology*, *2019*, 1–9.
7. Sharma, D., Kanchi, S., & Bisetty, K. (2019). Biogenic synthesis of nanoparticles: A review. *Arabian Journal of Chemistry*, *12*(8), 3576–3600.
8. Sharma, V. K., Yngard, R. A., & Lin, Y. (2009). Silver nanoparticles: Green synthesis and their antimicrobial activities. *Advances in Colloid and Interface Science*, *145*, 83–96.
9. Singh, P., Kim, Y. J., Zhang, D., & Yang, D. C. (2016). Biological synthesis of nanoparticles from plants and microorganisms. *Trends in Biotechnology*, *34*, 588–599.
10. Nasrollahzadeh, M., Sajadi, S. M., Issaabadi, Z., & Sajjadi, M. (2019). Biological sources used in green nanotechnology. *Interface Science and Technology*, *28*, 81–111.
11. Dahoumane, S. A., Mechouet, M., Alvarez, F. J., Agathos, S. N., & Jeffryes, C. (2016). Microalgae: An outstanding tool in nanotechnology. *Bionatura*, *1*, 196–201.
12. Leaf, M. C., Gay, J. S. A., Newbould, M. J., Hewitt, O. R., & Rogers, S. L. (2020). Calcareous algae and cyanobacteria. *Geology Today*, *36*, 75–80.
13. Borowitzka, M. A. (2013). High-value products from microalgae-their development and commercialisation. *Journal of Applied Phycology*, *25*, 743–756.
14. Gahlawat, G., & Choudhury, A. R. (2019). A review on the biosynthesis of metal and metal salt nanoparticles by microbes. *RSC Advances*, *9*, 12944–12967.
15. Fawcett, D., Verduin, J. J., Shah, M., Sharma, S. B., & Poinern, G. E. J. (2017). A review of current research into the biogenic synthesis of metal and metal oxide nanoparticles via marine algae and seagrasses. *Journal of Nanoscience*, *2017*, 1–15.
16. Ponnuchamy, K., & Jacob, J. A. (2016). Metal nanoparticles from marine seaweeds—A review. *Nanotechnology Reviews*, *5*, 589–600.
17. Katata-Seru, L., Moremedi, T., Aremu, O. S., & Bahadur, I. (2018). Green synthesis of iron nanoparticles using *Moringa oleifera* extracts and their applications: Removal of nitrate from water and antibacterial activity against *Escherichia coli*. *Journal of Molecular Liquids*, *256*, 296–304.
18. Segneanu, A. E., Orbeci, C., Lazau, C., Sfirloaga, P., Vlazan, P., Bandas, C., & Grozescu, I. (2013). Waste water treatment methods. In: W. Elshorbagy & R.K. Chowdhury (Eds.), *Water treatment* (pp. 53–80). InTech Publishing.
19. Grassi, M., Kaykioglu, G., Belgiorno, V., & Lofrano, G. (2012). Removal of emerging contaminants from water and wastewater by adsorption process. emerging compounds removal from wastewater: Natural and solar based treatments. In: G. Lofrano (Ed.), *Springer briefs in green chemistry for sustainability* (pp. 15–37). Springer.
20. Larsson, D. G. J., Pedro, C., & Paxeus, N. (2007). Effluent from drug manufactures contains extremely high levels of pharmaceuticals. *Journal of Hazardous Materials*, *148*, 751–755.
21. Jjemba, P. K. (2006). Excretion and ecotoxicity of pharmaceutical and personal care products in the environment. *Ecotoxicology and Environmental Safety*, *63*, 113–130.
22. Lienert, J., Güdel, K., & Escher, B. I. (2007). Screening method for ecotoxicological hazard assessment of 42 pharmaceuticals considering human metabolism and excretory routes. *Environmental Science & Technology*, *41*, 4471–4478.
23. Peng, X., Tang, C., Yu, Y., Tan, J., Huang, Q., Wu, J., Chen, S., & Mai, B. (2009). Concentrations, transport, fate, and releases of polybrominated diphenyl ethers in sewage treatment plants in the Pearl River Delta, South China. *Environment International*, *35*(2), 303–309.
24. Yu, F., Li, Y., Han, S., & Ma, J. (2016). Adsorptive removal of antibiotics from aqueous solution using carbon materials. *Chemosphere*, *153*, 365–385.
25. Górny, D., Guzik, U., Hupert-Kocurek, K., & Wojcieszyńska, D. (2019). Naproxen ecotoxicity and biodegradation by *Bacillus thuringiensis* B1(2015b) strain. *Ecotoxicology and Environmental Safety*, *167*, 505–512.
26. Ding, T., Lin, K., Yang, B., Yang, M., Li, J., Li, W., & Gan, J. (2017). Biodegradation of naproxen by freshwater algae *Cymbella* sp. and

Scenedesmus quadricauda and the comparative toxicity. *Bioresource Technology*, *238*, 164–173.
27. de Lima Barizão, A. C., Silva, M. F., Andrade, M., Brito, F. C., Gomes, R. G., & Bergamasco, R. (2020). Green synthesis of iron oxide nanoparticles for tartrazine and bordeaux red dye removal. *Journal of Environmental Chemical Engineering*, *8*(1), 103618.
28. Jaafar, S. N. B. S. (2006). Adsorption study-dye removal using clay. BSc Thesis, Faculty of Chemical Engineering and Natural Resources. University College of Engineering & Technology Malaysia, Johor Bahru, Johor, Malaysia.
29. Kumar, R., Rashid, J., & Barakat, M. A. (2014). Synthesis and characterization of a starch-AlOOH-FeS_2 nanocomposite for the adsorption of congo red dye from aqueous solution. *RSC Advances*, *4*(72), 38334–38340.
30. Kyzas, G. Z., Lazaridis, N. K., & Mitropoulos, A. C. (2012). Removal of dyes from aqueous solutions with untreated coffee residues as potential low-cost adsorbents: Equilibrium, reuse and thermodynamic approach. *Chemical Engineering Journal*, *189*, 148–159.
31. Sahin, M., Arslan, Y., & Tomul, F. (2022). Adsorption, oxidation, kinetic and thermodynamic studies of methyl orange by magnetic Fe_3O_4 NPs and their chitosan/alginate nanocomposites. *International Journal of Environmental Analytical Chemistry*. https://doi.org/10.1080/03067319.2022.2140417
32. Tran, H. N., You, S.-J., & Chao, H.-P. (2016). Effect of pyrolysis temperatures and times on the adsorption of cadmium onto orange peel derived biochar. *Waste Management & Research: The Journal of the International Solid Wastes and Public Cleansing Association, Iswa*, *34*, 129–138.
33. Tran, H. N., Wang, Y.-F., You, S.-J., & Chao, H.-P. (2017). Insights into the mechanism of cationic dye adsorption on activated charcoal: the importance of π–π interactions. *Process Safety and Environmental Protection*, *107*, 168–180.
34. Cherif, W., Ktari, L., El Bour, M., Boudabous, A., & Grignon-Dubois, M. (2016). *Codium fragile* subsp. fragile (Suringar) Hariot in Tunisia: Morphological data and status of knowledge. *ALGAE*, *31*(2), 129–136.
35. Nishanthi, R., Malathi, S., John Paul, S., & Palani, P. (2019). Green synthesis and characterization of bioinspired silver, gold and platinum nanoparticles and evaluation of their synergistic antibacterial activity after combining with different classes of antibiotics. *Materials Science & Engineering, C: Biomimetic and Supramolecular Systems*, *96*, 693–707.
36. Sahin, M., & Gubbuk, I. H. (2019). Green synthesis of antioxidant silver and platinum nanoparticles using ginger and turmeric extracts and investigation of their catalytic activity. *Journal of the Turkish Chemical Society, Section A: Chemistry*, *6*(3), 403–410.
37. Kora, A. J., & Rastogi, L. (2018). Green synthesis of palladium nanoparticles using gum ghatti (*Anogeissus latifolia*) and its application as an antioxidant and catalyst. *Arabian Journal of Chemistry*, *11*, 1097–1106.
38. Lebaschi, S., Hekmati, M., & Veisi, H. (2017). Green synthesis of palladium nanoparticles mediated by black tea leaves (*Camellia sinensis*) extract: Catalytic activity in the reduction of 4-nitrophenol and Suzuki-Miyaura coupling reaction under ligand-free conditions. *Journal of Colloid & Interface Science*, *485*, 223–231.
39. Sahin, M., Arslan, Y., & Tomul, F. (2022). Removal of naproxen and diclofenac using magnetic nanoparticles/nanocomposites. *Research on Chemical Intermediates*, *48*, 5209–5226.
40. Kragović, M., Stojmenović, M., Petrović, J., Loredo, J., Pašalić, S., Nedeljković, A., & Ristović, I. (2019). Influence of alginate encapsulation on point of zero charge (pHpzc) and thermodynamic properties of the natural and Fe(III)-modified zeolite. *Procedia Manufacturing*, *32*, 286–293.
41. Bharath, G., Alhseinat, E., Ponpandian, N., Khan, M. A., Siddiqui, M. R., Ahmed, F., & Alsharaeh, E. H. (2017). Development of adsorption and electrosorption techniques for removal of organic and inorganic pollutants from wastewater using novel magnetite/porous graphene-based nanocomposites. *Separation and Purification Technology*, *188*, 206–218.
42. Fytianos, K., Voudrias, E., & Kokkalis, E. (2000). Sorption-desorption behaviour of 2,4-dichlorophenol by marine sediments. *Chemosphere*, *40*(1), 3–6.
43. Paluri, P., Ahmad, K. A., & Durbha, K. S. (2022). Importance of estimation of optimum isotherm model parameters for adsorption of methylene blue onto biomass derived activated carbons: Comparison between linear and non-linear methods. *Biomass Conversion and Biorefinery*, *12*, 4031–4048.
44. Harrache, Z., Abbas, M., Aksil, T., & Trari, M. (2019). Thermodynamic and kinetics studies on adsorption of indigo carmine from aqueous solution by activated carbon. *Microchemical Journal*, *144*, 180–189.
45. Ravikumar, K. V. G., Sudakaran, S. V., Ravichandran, K., Pulimi, M., Natarajan, C., & Mukherjee, A. (2019). Green synthesis of NiFe nano particles using punica granatum peel extract for tetracycline removal. *Journal of Cleaner Production*, *210*, 767–776.
46. Sahin, M., & Arslan, Y. (2023). Adsorptive and oxidative removal of naproxen and diclofenac using Ag NPs, Cu NPs and Ag/Cu NPs. *Research on Chemical Intermediates*, *49*, 3627–3643. https://doi.org/10.1007/s11164-023-05048-w
47. Khazri, H., Ghorbel-Abid, I., Kalfat, R., & Ayadi, M. (2017). Removal of ibuprofen, naproxen and carbamazapine in aqueous solution onto natural clay: Equilibrium, kinetics, and thermodynamic study. *Applied Water Science*, *7*(6), 3031–3040.
48. Malakootian, M., Mansoorian, H. J., Hosseini, A., & Khanjani, N. (2015). Evaluating the efficacy of alumina/carbon nanotube hybrid adsorbents in removing Azo Reactive Red 198 and Blue 19 dyes from aqueous solutions. *Process Safety and Environment Protection*, *96*, 125–137.
49. Annadurai, G., Juang, R. S., & Lee, D. J. (2002). Use of cellulose-based wastes for adsorption of dyes from aqueous solutions. *Journal of Hazardous Materials*, *92*(3), 263–274.
50. Robati, D., Mirza, B., Rajabi, M., Moradi, O., Tyagi, I., Agarwal, S., & Gupta, V. K. (2016). Removal of hazardous dyes-BR 12 and methyl orange using graphene oxide as an adsorbent from aqueous phase. *Chemical Engineering Journal*, *284*, 687–697.

SUPPORTING INFORMATION

Additional supporting information can be found online in the Supporting Information section at the end of this article.

How to cite this article: Şahin, M., Arslan, Y., Tomul, F., Akgül, F., & Akgül, R. (2024). Green synthesis of metal nanoparticles from *Codium macroalgae* for wastewater pollutants removal by adsorption. *CLEAN – Soil, Air, Water*, *52*, e2300187. https://doi.org/10.1002/clen.202300187